Stability of a liquid-metal layer between gas streams with and without a magnetic field

Laurent Martin Witkowski and Philippe Marty[a)]
Laboratoire LEGI, BP 53 X, F-38041 Grenoble Cedex, France

(Received 14 April 1997; accepted 21 July 1997)

The linear stability of a plane liquid sheet of metal flowing between parallel gas streams having different velocities is considered. The presence of a magnetic field only slightly modifies the neutral stability curves obtained in the hydrodynamic regime where Kelvin–Helmholtz instabilities are the dominant mechanism in the destabilization of the sheet. The most unstable wavelength is found to scale with We^{-1} where We is the Weber number. As expected, the growth rate of the instabilities is decreased when a transverse magnetic field is applied. However, the growth rate is increased when the applied magnetic field is parallel to the direction of the velocities. A possible explanation of this unusual phenomenon is presented. In an experimental air-blast atomizer with water and nitrogen, particle size and velocity measurements have been made with a laser-doppler analyzer. The results agree with the theoretical predictions for zero magnetic flux density and are also consistent with predictions based on a more global breakup mechanism. © *1997 American Institute of Physics.* [S1070-6631(97)00912-4]

I. INTRODUCTION

The effect of magnetohydrodynamic forces on the interface between two electrically conducting fluids has been investigated by many authors. Most of these studies focused on metallurgical situations where high intensity electric currents cross one or possibly several liquid/liquid or liquid/solid boundaries. For example, in a stability study of electric arc furnaces, Sneyd[1] used a model with three liquid layers, each with a different density and electrical conductivity, and with a steady (direct) electric current perpendicular to the interfaces. Similar models have been used in attempts to design larger aluminum reduction cells where the need to avoid oscillations of the interface between the cryolith layer and the melted aluminum severely limits cell size.[2,3] All these studies illustrated the competing roles of Lorentz forces, gravity, surface tension, and inertia in interfacial instabilities. Recent attempts to reduce size variations in metallic powders obtained by gas atomization of conical liquid-metal sheets have clearly shown the sheets must remain axisymmetric and stable prior to the impingement of the external coaxial gas streams (Fig. 1).

The stability of a liquid-metal sheet without an externally applied magnetic field has been investigated both analytically and experimentally as a function of the initial thickness, angular velocity, and other physical or geometrical aspects.[4] The results show that it was quite easy to maintain the coherence of the liquid sheet between its birth at the nozzle outlet and the region (referred to as the active zone in Fig. 1) where the gas jets start the atomization process, as long as the distance between the nozzle and active zone is roughly 10–20 cm. However, for some technologically important applications, this distance must be much larger. In such a case, one must ensure that the sheet reaches the active zone without instabilities that would lead to the formation of big droplets which cannot be disintegrated into small droplets by the jets. One way to achieve the required sheet stability is to apply a magnetic field which is generally known to reduce the growth rate of any perturbations.[5] The aim of this paper is to investigate such a possibility. A linear stability study is presented in Sec. II with a discussion of the results in Sec. III. Although no experiments have been conducted with a magnetic field, experiments with water and air have been undertaken and the results presented in Sec. IV agree well with the model predictions for zero magnetic flux density. Validation of the model without a magnetic field provides some confidence in its predictions of magnetic field effects.

II. LINEAR STABILITY ANALYSIS

Since its curvature is small, the conical sheet can be treated as a plane two-dimensional liquid-metal layer with a thickness of $2a$. For the actual situation shown in Fig. 1, the gas velocity inside the sheet is almost zero. However, for the sake of generality, we assume that the liquid-metal layer is sandwiched between two parallel gas flows (Fig. 2). The electrical conductivity of the liquid metal is σ, while ρ_m and ρ_g are the densities of the metal and the gas, respectively. This study only considers a steady uniform magnetic field which is either perpendicular or parallel to the flow direction.

For a linear stability analysis, the positions of the two interfaces are given by

$$z=\eta_1=-a+Ae^{i(qx-\omega t)+i\Phi}, \tag{1a}$$

$$z=\eta_2=a+Ae^{i(qx-\omega t)}, \tag{1b}$$

where A is real and represents the small interfacial displacement from $z=a$ while Φ is complex and allows the interface near $z=-a$ to have a different amplitude and phase than that near $z=+a$. The real wave number of the perturbation is q, while $\omega=\omega_r+i\omega_i$, where ω_r is the circular frequency and ω_i is the amplification factor. Neglecting the viscous effects in the three layers, the x and z components of the momentum equation, together with continuity, become

a)Electronic mail: Philippe.Marty@hmg.inpg.fr

 1070-6631/97/9(12)/3707/11/$10.00

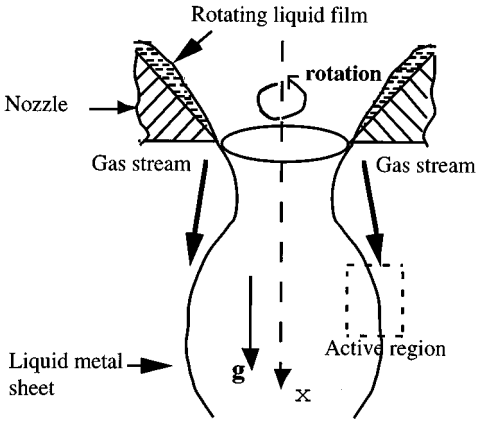

FIG. 1. The electromagnetic atomizer: the liquid metal flow is transformed into an annular sheet prior to its disintegration by a neutral gas stream.

$$-i\omega\rho_j u_j + iq\rho_j U_j u_j = -iqp_j + \epsilon_j F(B_\perp), \tag{2a}$$

$$-i\omega\rho_j w_j + iq\rho_j U_j w_j = -Dp_j + \epsilon_j F(B_\parallel) + \rho_j g, \tag{2b}$$

$$iqu_j + Dw_j = 0, \tag{2c}$$

where $D=\partial/\partial z$, U_j is the unperturbed velocity in the layer j ($j=0,1,2$), and $(u_j,0,w_j)$ is the velocity perturbation while $\epsilon_j=1$ for $j=0$ and $\epsilon_j=0$ for $j=1$ or 2. The density ρ_j is equal to ρ_m for $j=0$ and to ρ_g for $j=1$ or 2, while g denotes the gravitational acceleration.

There is a magnetohydrodynamic (MHD) force opposing the motion across the magnetic field,

$$F(B_\perp) = -\sigma(U_0+u_0)B_\perp^2, \tag{3a}$$

$$F(B_\parallel) = -\sigma w_0 B_\parallel^2 \tag{3b}$$

in Eq. (2a) or (2b) for a perpendicular or parallel magnetic field, respectively. Equation (3a) includes the MHD opposition to the unperturbed velocity and the axial velocity perturbation with a perpendicular magnetic field. Since the conical sheet is axisymmetric, the azimuthal gradient of the electric potential is zero and no electric field appears in Eqs. (3). For an actual plane layer, any short-circuiting of the liquid-metal layer through an infinitely conducting wall would also cancel the y derivative of the potential and, consequently, would also lead to the same equation. Eliminating p and u in Eqs. (2) yields a simple equation for the vertical velocity perturbation w:

$$D^2w - Q^2w = 0 \quad \text{in the metal}, \tag{4a}$$

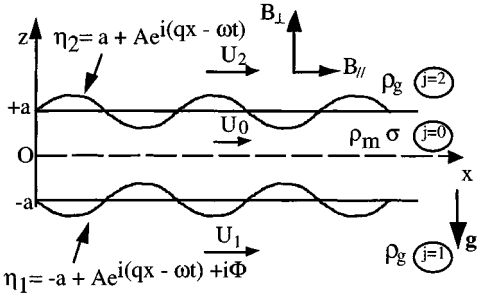

FIG. 2. Mathematical model and notations.

$$D^2w - q^2w = 0 \quad \text{in the gas}, \tag{4b}$$

where the complex quantity Q is

$$Q^2 = Q_\parallel^2 = q^2\left[1 + i\,\frac{\sigma B_\parallel^2}{\rho_m(\omega - U_0 q)}\right] \quad \text{if } B=B_\parallel, \tag{5a}$$

$$Q^2 = Q_\perp^2 = q^2\left[1 + i\,\frac{\sigma B_\perp^2}{\rho_m(\omega - U_0 q)}\right]^{-1} \quad \text{if } B=B_\perp. \tag{5b}$$

Equations (4) are solved with the conditions that w and Dw are continuous at the gas–metal interfaces and that $w\to 0$ as $z\to\pm\infty$. Equation (2c) then gives u. For brevity, we only present u and w in the liquid metal:

$$u_0 = (\omega - U_0 q)\left(\frac{e^{Qa}-e^{i\phi}e^{-Qa}}{e^{2Qa}-e^{-2Qa}}\,e^{Qz} - \frac{e^{Qa+i\phi}-e^{-Qa}}{e^{2Qa}-e^{-2Qa}}\,e^{-Qz}\right)\frac{Q}{q}\,Ae^{i(qx-\omega t)}, \tag{6a}$$

$$w_0 = -i(\omega - U_0 q)\left(\frac{e^{Qa}-e^{i\phi}e^{-Qa}}{e^{2Qa}-e^{-2Qa}}\,e^{Qz} + \frac{e^{Qa+i\phi}-e^{-Qa}}{e^{2Qa}-e^{-2Qa}}\,e^{-Qz}\right)Ae^{i(qx-\omega t)}. \tag{6b}$$

The solution for p in the gases and liquid metal are obtained by substituting the solutions for u and w into Eq. (2a). Equating the pressure jump across each interface to the surface tension γ times the local curvature of the interface positions given by Eqs. (1) gives two equations whose sum and difference are

$$\frac{\rho_g}{q}\left[(\omega - U_2 q)^2 + (\omega - U_1 q)^2 e^{i\Phi}\right] + \frac{\rho_m}{Q}(\omega - U_0 q)^2\tanh(Qa)(1+e^{i\Phi}) = \gamma q^2(1+e^{i\Phi}) + \Delta\rho g(1-e^{i\Phi}), \tag{7a}$$

$$\frac{\rho_g}{q}\left[(\omega - U_2 q)^2 - (\omega - U_1 q)^2 e^{i\Phi}\right] + \frac{\rho_m}{Q}(\omega - U_0 q)^2\coth(Qa)(1-e^{i\Phi}) = \gamma q^2(1-e^{i\Phi}) + \Delta\rho g(1+e^{i\Phi}), \tag{7b}$$

where $\Delta\rho=\rho_m-\rho_g$ is the density difference between the liquid metal and the gas. Equations (7) can be simplified by introducing the dimensionless quantities:

$$\rho = \frac{\rho_m}{\rho_g}, \quad k = qa, \quad \Omega = \frac{\omega a}{U_0}, \quad V_1 = \frac{U_1}{U_0}, \quad V_2 = \frac{U_2}{U_0},$$
$$\mathrm{We} = \frac{\rho_g U_0^2 a}{\gamma}, \quad \mathrm{Fr} = \frac{\rho_g U_0^2}{\Delta\rho g a}, \quad N = \frac{\sigma B^2 a}{\rho_m U_0},$$
$$K = Qa = k\left(1 + i\,\frac{N}{\Omega - k}\right)^n$$
$$\text{with } n = +1/2 \text{ if } B=B_\parallel \text{ and } n=-1/2 \text{ if } B=B_\perp, \tag{8}$$

where the liquid film thickness and velocity have been used as characteristic quantities, We and Fr are the Weber and

Froude numbers, and N is the magnetic interaction parameter which is the characteristic ratio of the electromagnetic forces to inertial forces.

The dimensionless version of Eqs. (7) are:

$$\frac{1}{k}\left[(\Omega - V_2 k)^2 + (\Omega - V_1 k)^2 e^{i\Phi}\right] + \frac{\rho}{K}(\Omega - k)^2$$

$$\tanh(K)(1+e^{i\Phi}) = \frac{k^2}{\mathrm{We}}(1+e^{i\Phi}) + \frac{1}{\mathrm{Fr}}(1-e^{i\Phi}), \qquad (9a)$$

$$\frac{1}{k}\left[(\Omega - V_2 k)^2 - (\Omega - V_1 k)^2 e^{i\Phi}\right] + \frac{\rho}{K}(\Omega - k)^2$$

$$\coth(K)(1-e^{i\Phi}) = \frac{k^2}{\mathrm{We}}(1-e^{i\Phi}) + \frac{1}{\mathrm{Fr}}(1+e^{i\Phi}). \qquad (9b)$$

Eliminating Φ in Eqs. (9a) and (9b) yields the characteristic equation

$$\alpha_4 \Omega^4 + \alpha_3 \Omega^3 + \alpha_2 \Omega^2 + \alpha_1 \Omega + \alpha_0 = 0, \qquad (10)$$

where the coefficients $\alpha_i = f_i(\rho, k, K, V_1, V_2, \mathrm{We}, \mathrm{Fr})$ for $i = 0,1,2,3,4$ are given in the Appendix. For a given wave number k, the critical gas velocity which triggers the instability is found by progressively increasing the value of V_1 (or V_2) until the dimensionless amplification factor Ω_i, becomes positive. Without a magnetic field, K is real and is equal to k, and the coefficients α_i are also real: in this case, Eq. (10) is a simple fourth-order polynomial with two pairs of conjugated roots. As $k \to \infty$, the sum and the difference of Eqs. (9a) and (9b) simplify to the equations for the classical Kelvin–Helmholtz instability. On the other hand, with a magnetic field, K is a complex number and depends on Ω, so that Eq. (10) is not a simple polynomial. We use an iterative Newton–Raphson scheme to solve Eq. (10) beginning with the four roots for $B=0$ and $K=k$.

III. RESULTS

First, we consider the values of the dimensionless parameters for practical applications. Since we are investigating a liquid sheet flowing between gas streams, we assume that $\rho \gg 1$. For liquid steel atomized by nitrogen, or water in air, $\rho = 5600$ or 800, respectively. In most of the laboratory or even industrial applications concerned with gas atomization, the Froude number is also very large and the effects of gravity can be ignored. For example, $\mathrm{Fr} = 122$ for a 0.1-mm-thick layer of water flowing at 10 m/s in a nitrogen atmosphere. For liquid steel in nitrogen, $\mathrm{Fr} = 17$, which is large enough to neglect gravitational effects. For the same velocity and thickness the Weber number would be 0.17 for water and 0.02 for a liquid metal such as mercury. Large values of We can nevertheless be obtained with thick liquid metal layers and high speeds. The interaction parameter $N = 0.15$ for a 1-mm-thick layer of liquid steel flowing at 0.1 m/s in a magnetic field of 1 T. Under the same conditions, for sodium, $N = 12.5$.

A. Without a magnetic field ($N=0$)

We begin with equal gas velocities ($V_1 = V_2$). Figure 3 shows that the sinuous mode $\Phi_r = 0$ has a higher growth rate

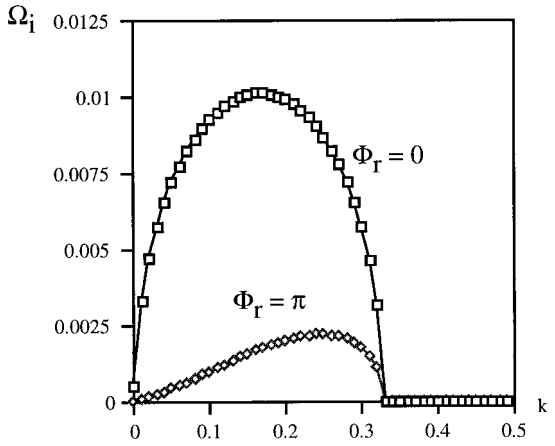

FIG. 3. Liquid sheet flowing in a gas atmosphere at rest ($V_1 = V_2 = 0$): comparison between the growth rates of the sinuous mode ($\Phi_r = 0$) and of the varicose mode ($\Phi_r = \pi$) for $\mathrm{We} = 0.33$, $\rho = 800$ and $\mathrm{Fr} \gg 1$.

than the varicose mode $\Phi_r = \pi$, where Φ_r is the real part of the phase shift between the two interfaces. In both cases $\Phi_i = 0$, so that $\Phi = 0$ at neutral stability. The dominance of the sinuous mode is confirmed by the behavior of the water sheet in Fig. 4 and by previous works of Hagerty and Shea,[6] who considered equal velocity gas streams.

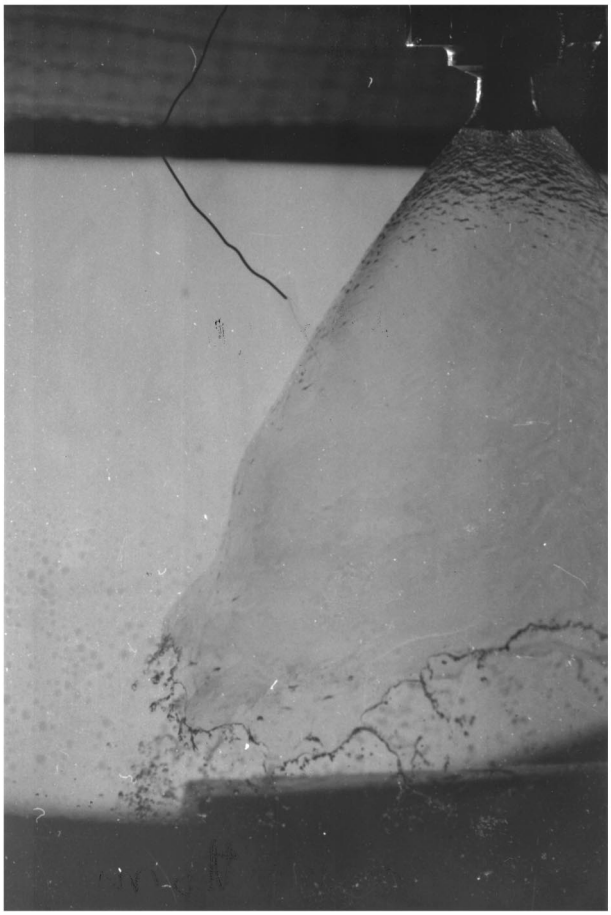

FIG. 4. Growing of the sinuous mode of a water sheet flowing at 5 m/s in air ($\mathrm{We} = 13$).

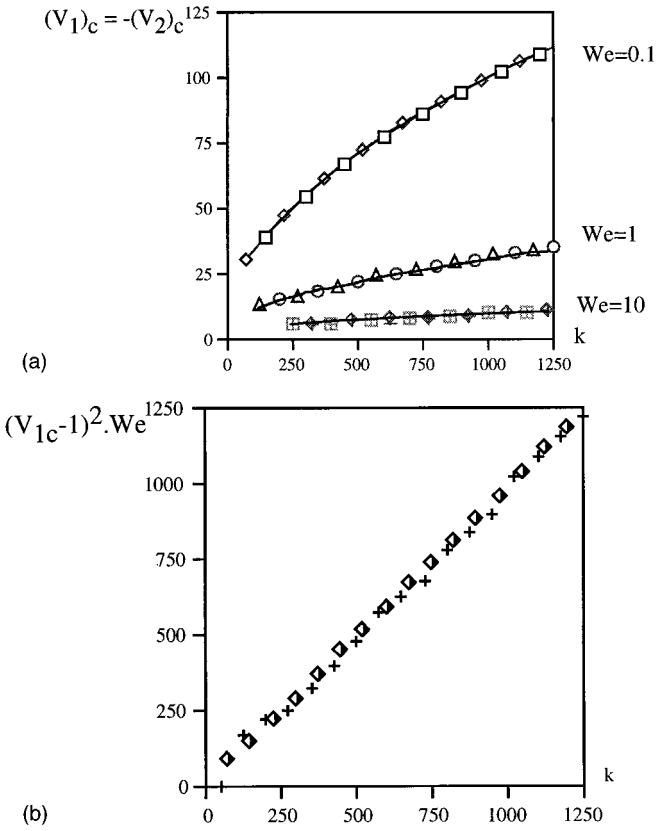

FIG. 5. Liquid sheet flowing between gas streams having opposite directions ($V_1 = -V_2$) for We=0.1, 1, and 10, $\rho = 5600$, and Fr$\gg 1$: (a) evolution of the critical velocities of the gas flows vs k. (b) Linear dependence of the quantity $\Delta V_c^2 \cdot$We with k.

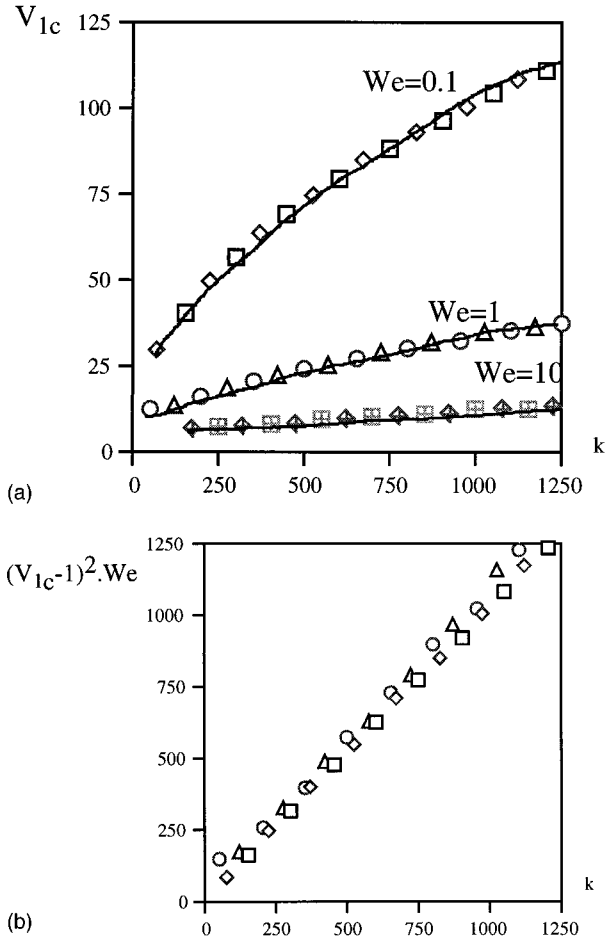

FIG. 6. Liquid sheet flowing between a gas stream of velocity V_1 and a gas atmosphere at rest ($V_2 = 0$) for We=0.1, 1, and 10, $\rho = 5600$, and Fr$\gg 1$: (a) evolution of the critical velocity V_{1c} of the gas vs k. (b) Linear dependence of the quantity $\Delta V_c^2 \cdot$We with k.

When two gas jets with high but unequal velocities flow beside a lower velocity liquid-metal sheet, $\rho \gg 1$, $V_1 \gg 1$, $V_2 \gg 1$, and $V_1 \neq V_2$, then at the critical velocity there is an equilibrium in the direction normal to the sheet between pressure forces created by the gas flows and surface tension forces opposing the deformation of the interface. Using dimensional quantities, a simple estimation of this equilibrium gives

$$\rho_g (\Delta U)_c^2 \approx \gamma q, \tag{11}$$

where $(\Delta U)_c$ is the critical difference of velocities between the liquid sheet and the gas stream. Using the dimensionless quantities defined in Eqs. (8), Eq. (11) becomes

$$(\Delta V)_c^2 \mathrm{We} = k. \tag{12}$$

This simple way of estimating the critical velocity has been successfully verified. For two gas streams flowing with equal velocities in opposite directions ($V_1 = -V_2$), the critical velocity $(V_1)_c$ is plotted in Fig. 5 as a function of k for various values of We and for Fr$\gg 1$. Equation (12) is confirmed by the plot of $(V_{1c}-1)^2$We vs k in Fig. 5(b). While Figs. 5(a) and 5(b) assume that $\rho = 5600$, i.e., steel in nitrogen, calculations for other values of ρ verify that the dimensionless critical velocity is independent of ρ as long as $\rho \gg 1$. Some industrial situations can require that only one side of the liquid sheet is exposed to a gas stream. In Fig. 6, the critical value of V_1 vs k is plotted for $V_2 = 0$.

The results are quite similar to those in Fig. 5, indicating that the significant velocity difference to be used in Eq. (12) is

$$\Delta V = \max(V_1, V_2) - 1. \tag{13}$$

This statement agrees with results of Panchagnula *et al.*[7] for the three-dimensional stability of an annular liquid sheet subjected to different gas velocities on opposite sides. Equation (12) also agrees with the predictions of stability study for a viscous liquid curtain falling under gravity in an ambient gas[8] where the wave number for the maximum convective instability in the sinuous mode scaled with a quantity denoted by Q/We, which equals $\rho_g U^2/\gamma$ in our notation. In this study,[8] the Reynolds number of the liquid curtain was Re=5000, and the role of viscosity was very small. In all the situations discussed above, the phase velocity of the instabilities is equal to that of the liquid sheet, or, in dimensionless form

$$\Omega_r \approx k. \tag{14}$$

This result is confirmed by the results presented in Figs. 7(a) and 7(b) and indicates that the phase velocity of the

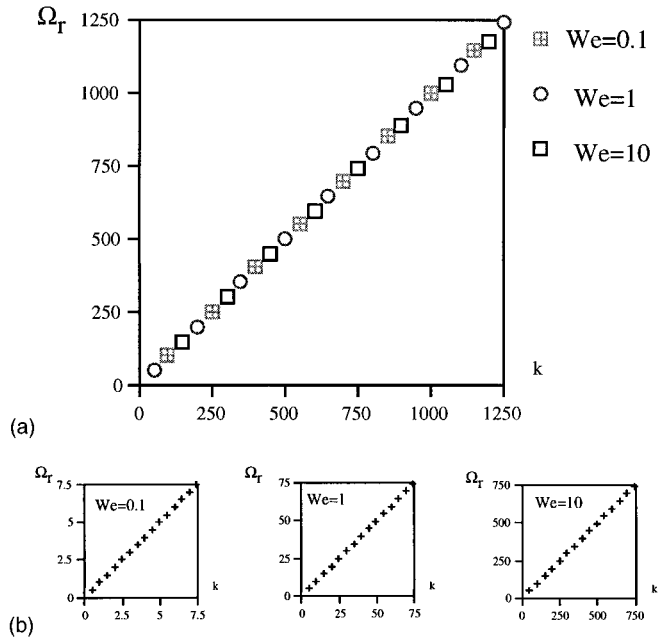

FIG. 7. Phase velocity of the instability vs k for We$=0.1$, 1, and 10, $\rho \gg 1$, and Fr$\gg 1$ (a) $V_1=-V_2$. (b) $V_1=0$, $V_2=10$.

instability is almost equal to that of the liquid sheet, even for nonsymmetric situations such as $V_1=-V_2$ or $V_1=0$, $V_2=10$.

We now focus on the behavior of the growth rate, Ω_i, of the instability. Ignoring gravitational effects by imposing Fr$\gg 1$, Fig. 8 shows the evolution of Ω_i vs k/We for various values of We for the case of a liquid sheet flowing in a gas at rest ($V_1=V_2=0$). We see that increasing We leads to an increase of the dimensionless growth rate. In order to understand this tendency, it would be helpful to study the values of the maximum amplification rate of the instability, $\Omega_{i\max}$, and of the associated wave number $k_{\max}$. Taking advantage of the previously discussed result that $\Phi=0$ for the most unstable perturbations, the stability of this problem can be described by a single equation:

$$\Omega^2+\rho(\Omega-k)^2\ \tanh(k)=\frac{k^3}{\mathrm{We}} \tag{15}$$

with solutions

$$\Omega_r=\frac{\rho k\ \tanh(k)}{1+\rho\ \tanh(k)}, \tag{16a}$$

$$\Omega_i=\frac{\sqrt{\dfrac{k^3}{\mathrm{We}}\ (1+\rho\ \tanh(k))-\rho k^2\ \tanh(k)}}{1+\rho\ \tanh(k)}. \tag{16b}$$

When $\tanh(k)\gg 1/\rho$, this solution becomes:

$$\Omega_r=k, \tag{17a}$$

$$\Omega_i=\sqrt{\frac{\dfrac{k^3}{\mathrm{We}}-k^2}{\rho\ \tanh(k)}}, \tag{17b}$$

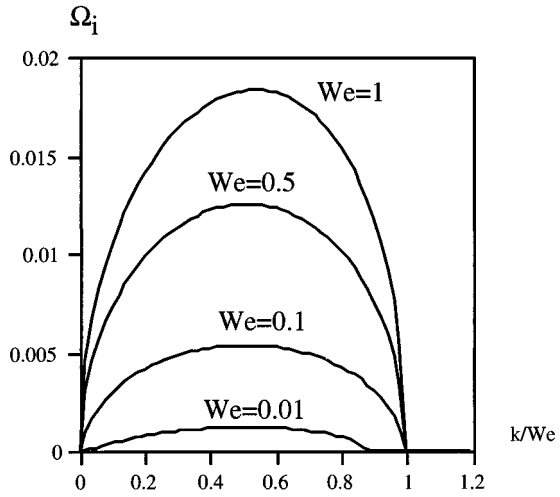

FIG. 8. Growth rate evolution vs k in the symmetric case $V_1=V_2=0$ for We$=0.01$, 0.1, 0.5, and 1. $\rho=800$, Fr$\gg 1$, $N=0$.

which is the dimensionless formulation of the solution proposed by Hagerty and Shea.[6] The expression obtained for Ω_i confirms that the cutoff wave number $k_c=\mathrm{We}$. In two asymptotic limits, Eq. (16) yields simple expressions for $\Omega_{i\ \max}$, which are presented in Table I.

(1) For $\tanh(k)\sim 1$, which is true for $\mathrm{We}(\Delta V)^2\gg 1$,

$$\Omega_{i\ \max}=\frac{2}{3\sqrt{3}}\ \frac{\mathrm{We}}{\sqrt{\rho}}\ (\Delta V)^3, \tag{18a}$$

$$k_{\max}=\tfrac{2}{3}\mathrm{We}(\Delta V)^2. \tag{18b}$$

(2) For $1/\rho\ll k\ll 1$, which is equivalent to $1/\rho \ll \mathrm{We}(\Delta V)^2\ll 1$,

$$\Omega_{i\ \max}=\frac{1}{2}\ \sqrt{\frac{\mathrm{We}}{\rho}}\ (\Delta V)^2, \tag{19a}$$

$$k_{\max}=\tfrac{1}{2}\mathrm{We}(\Delta V)^2. \tag{19b}$$

This second restriction on the value of k ($1/\rho\ll k\ll 1$) is in fact commonly satisfied in liquid rocket propulsion systems or in spray atomization for metallurgical, chemical, or agricultural purposes. The exact values of $\Omega_{i\ \max}$ and $k_{\max}$ have been numerically computed for $V_1=V_2=0$, $\rho=800$, and $\mathrm{We}=10^{-2}-10^3$, and the results are plotted in Fig. 9.

There is excellent agreement of $\Omega_{i\ \max}$ and $k_{\max}$ with the asymptotic results presented in Eqs. (18) and (19).

The nonsymmetric situation where only one side of the sheet is subjected to a gas stream has been also studied for values of (V_1,V_2), respectively, equal to (0,4) and (0,10). In the first case (Fig. 10), plotting Ω_i/We instead of Ω_i vs k/We reveals a particular crossing point, P, for which we have not yet found a satisfactory explanation. It is worth noting that the general shapes of the curves shown in Fig. 10 are exactly the same as those found for an annular sheet by Panchagnula *et al.*[7] (see Fig. 3 in this paper). For the second set of values of (V_1,V_2), Fig. 11 shows that the asymptotic expressions (18) and (19) of $\Omega_{i\ \max}$ are still valid despite the strong asymmetry of the situation. The slight disagreement around $\mathrm{We}(\Delta V)^2\sim 10^{-2}$ is probably due to the fact that $\mathrm{We}(\Delta V)^2$ is no longer much greater than $1/\rho=1.25\times 10^{-3}$.

TABLE I. Analytical expressions giving the most amplified regime ($k_{\max}$, $\Omega_{i\,\max}$) and the critical wave number k_c (for which $\Omega_i=0$) for a liquid metal sheet with equal gas velocities on its both sides. $\rho=\rho_m/\rho_g$ is assumed large compared to unity. ΔV denotes the dimensionless quantity $(U_{1,2}-U_0)/U_0=V_{1,2}-1$.

		$k_{\max}$	$\Omega_{i\,\max}$	k_c
$B=0$	$k\gg 1\Leftrightarrow \mathrm{We}(\Delta V)^2\gg 1$	$\frac{2}{3}\mathrm{We}(\Delta V)^2$	$\frac{2}{3\sqrt{3}}\frac{\mathrm{We}}{\sqrt{\rho}}(\Delta V)^3$	
	$\frac{1}{\rho}\ll k\ll 1\Leftrightarrow \frac{1}{\rho}\ll \mathrm{We}(\Delta V)^2\ll 1$	$\frac{1}{2}\mathrm{We}(\Delta V)^2$	$\frac{1}{2}\sqrt{\frac{\mathrm{We}}{\rho}}(\Delta V)^2$	
$B=B_{\parallel}$			$0.465\left(\frac{N\mathrm{We}^4}{\rho^2}(\Delta V)^{12}\right)^{1/5}$	$k_c=\mathrm{We}(\Delta V)^2$
$B=B_{\perp}$	$N\gg 1$ $k\gg 1\Leftrightarrow \mathrm{We}(\Delta)^2\gg 1$	$\frac{2}{3}\mathrm{We}(\Delta V)^2$	$0.28\left(\frac{\mathrm{We}^4}{N\rho^2}(\Delta V)^{12}\right)^{1/3}$	

Equation (17) agrees with the results of Squire[9] in a study of the stability of a thin axisymmetric conical sheet of fuel flowing in still air. The expressions (18) and (19) suggested for $k_{\max}$ and $\Omega_{i\,\max}$ have also been successfully used by Huang[10] in determining the breakup radius of a radially flowing axisymmetric sheet formed by the impingement of two coaxial water jets. Both Squire[9] and Huang[10] neglect viscous effects and obtain accurate results.

B. With a perpendicular or parallel magnetic field

The solutions of Eqs. (10) with the effects of a perpendicular or parallel field do not show any noticeable change in the value of the critical velocity, V_{1c}, of the gas flow. Moreover the velocity of the instabilities, Ω_r/k, is still very close to one for $\rho\gg 1$. Numerical tests have been performed for the situations studied in Figs. 6 and 7, but with a magnetic interaction parameter N equal to 10. No visible difference was observed when compared with $N=0$. The following heuristic explanation can be given to justify that the critical velocity is not affected by the magnetic field: when moving in the frame of reference with the liquid sheet, one can consider the critical threshold $\Omega_i=0$ as a static equilibrium between pressure forces and surface tension forces. Both of these forces are in

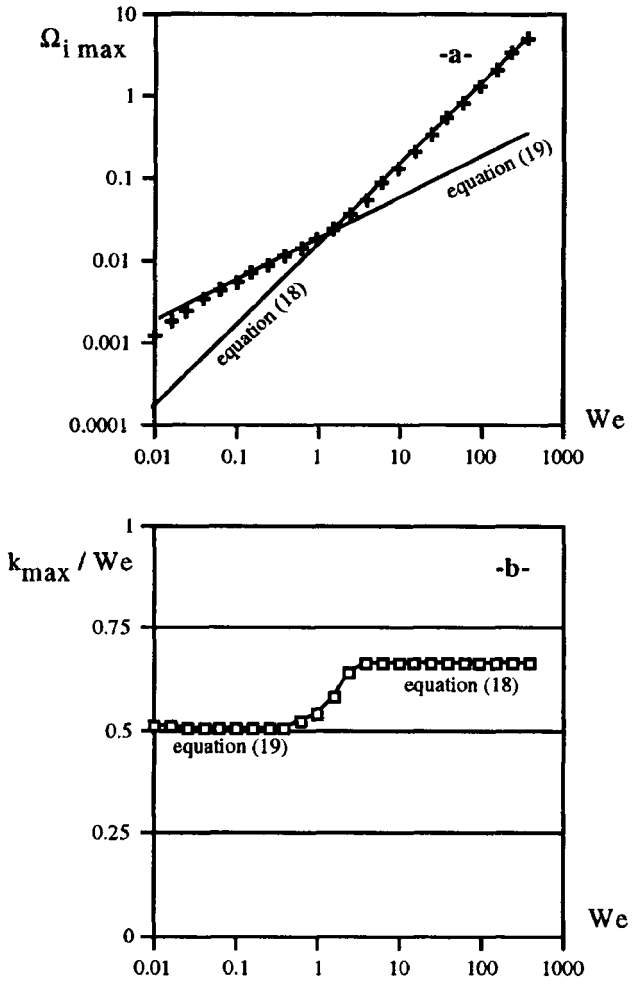

FIG. 9. Maximum growth rate $\Omega_{i\,\max}$ (a) and wave number of maximum amplification $k_{\max}$ (b) vs We in the symmetric case $V_1=V_2=0$ with $\rho=800$, $\mathrm{Fr}\gg 1$, $N=0$.

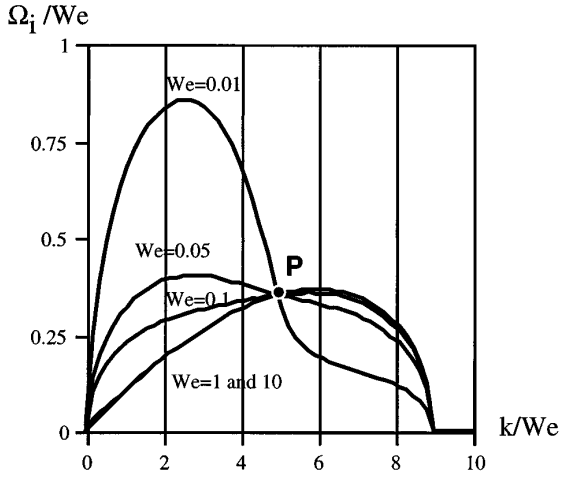

FIG. 10. Liquid sheet flowing between gas streams of different velocities ($V_1=0$, $V_2=4$): evolution of Ω_i/We vs k/We for $\mathrm{We}=0.01$, 0.05, 0.1, 1, and 10. $\rho=800$, $\mathrm{Fr}\gg 1$, $N=0$.

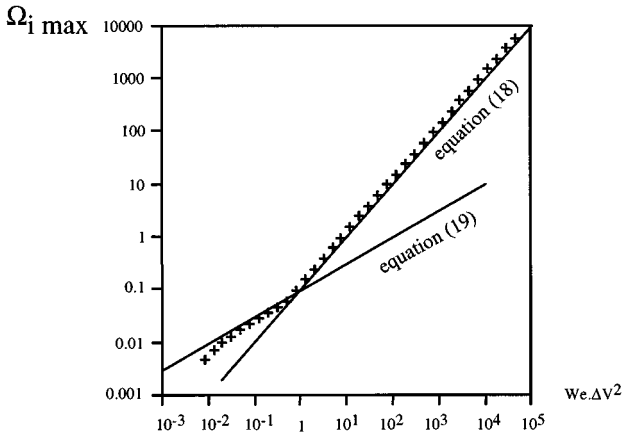

FIG. 11. Maximum growth rate $\Omega_{i\,\max}$ vs We ΔV^2 in a strongly nonsymmetric case: $V_1=0$ and $V_2=10$ ($\Delta V=V_2-1=9$). $\rho=800$, Fr$\gg 1$, $N=0$.

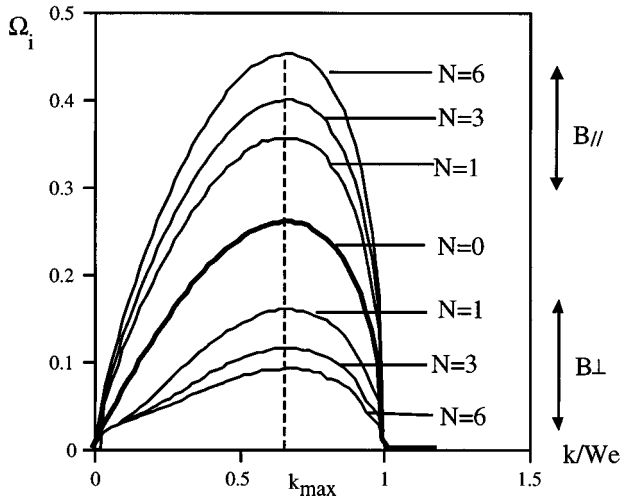

FIG. 12. Growth rate evolution vs k/We for various strengths and orientations of the magnetic field. We$=50$, $V_1=V_2=0$ ($\Delta V=1$), $\rho=5600$.

the z direction. When B is perpendicular to the sheet, the $J\times B$ product has no component in the z direction. Similarly, when B is parallel to the unperturbed sheet, only the velocities in the z direction would generate a force in this direction but such velocities are equal to zero when Ω_i equals zero. Another way to understand the inability of the magnetic field to modify the critical velocity is based on Eq. (6). At the instability threshold, i.e., when $\omega_i=0$, the first terms on the right-hand side of Eqs. (6) reduce to (ω_r-U_0q), which is zero when $\rho_g\ll\rho_m$. Consequently, w_0 vanishes and, from Eqs. (3), the MHD force $F(B_\parallel)$ in the z direction also vanishes, so that there is no influence of the magnetic field on the value of the critical velocity of the gas flow at which the instability occurs.

We now consider the effect of the magnetic field on the growth rate of the instability. The solutions for We$\gg 1$ provide a simple understanding of the stability problem. Such values of We can be obtained with thick liquid metal layers and high velocities. For a liquid sheet sandwiched between gas media at rest ($V_1=V_2=0$, and $\Delta V=1$), the most amplified wave number $k_{\max}$ is comparable to We and much larger than one, as indicated in Table I. This means that the wavelength of the growing mode will be much smaller than the sheet thickness. For large Weber numbers, the two interfaces are decoupled and satisfy a unique equation:

$$\frac{\Omega^2}{k}+\frac{\rho}{K}(\Omega-k)^2=\frac{k^2}{\mathrm{We}}. \tag{20}$$

In order to find an analytical solution of Eq. (20), we can take advantage of the numerical results concerning the wave velocity of the instabilities: $\Omega_r\sim k$. Moreover, for large values of N, the modified wave number K becomes

$$K\approx k\left[\frac{N}{\Omega_i}\right]^n, \tag{21}$$

where the fractional exponent n has been defined in Eq. (8). Equation (20) can be reduced further by comparing the order of magnitude of Ω_i and Ω_r. Without a magnetic field ($N=0$), this can be done by using the results of Table I. Forming the ratio $\Omega_{i\,\max}/\Omega_r$ gives

$$\frac{\Omega_{i\,\max}}{\Omega_r}=\frac{1}{\sqrt{3}}\frac{\Delta V}{\sqrt{\rho}}\quad\text{for}\ \ \mathrm{We}(\Delta V)^2\gg 1, \tag{22a}$$

$$\frac{\Omega_{i\,\max}}{\Omega_r}=\frac{1}{\sqrt{\rho\mathrm{We}}}\quad\text{for}\ \ \frac{1}{\rho}\ll\mathrm{We}(\Delta V)^2\ll 1. \tag{22b}$$

As an example, a 2-cm-thick steel layer flowing at 20 m/s in a nitrogen atmosphere at rest would give We$=50$ with the surface tension $\gamma=0.1$ N m^{-1}. For $\rho=5600$ the restriction of Eq. (22a) is satisfied and the ratio $\Omega_{i\,\max}/\Omega_r$ is found equal to 0.0077. We assume that $\Omega_{i\,\max}\ll\Omega_r$ with a magnetic field as well. This hypothesis will be confirmed later by the numerical results. Its introduction into Eq. (20) for asymptotic values of N ($N\gg 1$), gives the expression for the maximum growth rate of the instability with a transverse magnetic field:

$$\Omega_{i\,\max}=0.28\left(\frac{\mathrm{We}^4}{N\rho^2}(\Delta V)^{12}\right)^{1/3}\quad\text{when}\ \ B=B_\perp \tag{23}$$

or a parallel magnetic field:

$$\Omega_{i\,\max}=0.465\left(\frac{N\mathrm{We}^4}{\rho^2}(\Delta V)^{12}\right)^{1/5}\quad\text{when}\ \ B=B_\parallel. \tag{24}$$

In both cases, the wave number, $k_{\max}$ of maximum amplification is

$$k_{\max}=\tfrac{2}{3}\mathrm{We}(\Delta V)^2. \tag{25}$$

Equations (23) and (24) reveal the fundamental influence of the orientation of the magnetic field on the growth rate of the instability. A transverse field brakes the development of the instability, which is a rather classical result in MHD where dynamic phenomena are often slower when a magnetic field is applied. On the contrary, a parallel field seems to enhance the development of the instability. Figure 12 shows an illustration of the evolution of Ω_i vs k/We when $V_1=V_2=0$ and confirms the above results. For N varying between 0 and 6, the wave number $k_{\max}$ is found to be independent of N and of the direction of the magnetic field. This

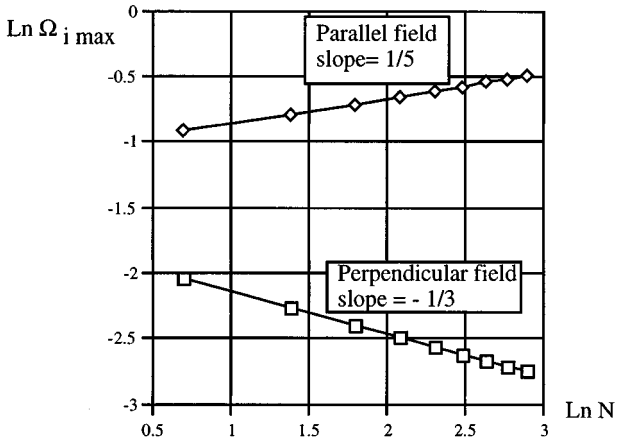

FIG. 13. Asymptotic dependence of $\Omega_{i\ \max}$ with N for We$=50$, $\rho=5600$, and $V_1=V_2=0$ $(\Delta V=1)$.

is in agreement with Eq. (25). The asymptotic behavior of $\Omega_{i\ \max}$ with N is shown in Fig. 13 and confirms Eqs. (23) and (24). Plots of the streamfunction of the velocity distribution in the metal [deduced from Eq. (6)], help in understanding this phenomena. Figure 14 shows, over one wavelength, the flow pattern without and with a magnetic field. For $N=0$, the depth of metal which is involved in the instability is of the order of k^{-1}, as already mentioned. When a perpendicular magnetic field is applied [Fig. 14(b)], the x-directed MHD force which brakes any movement along the x direction forces the streamlines to close deeper into the metal. Consequently, a larger amount of metal is dragged by the instability and inertial effects decrease the temporal growth rate. When a parallel magnetic field is applied [Fig. 14(c)], the streamlines are confined in a narrow ''hydrodynamic skin.'' This is a consequence of the Lorentz force in the z direction, which prevents a deep penetration of the flow into the liquid metal layer. In this case, a smaller amount of fluid is involved in the instability, thus decreasing inertial effects so that the growth rate increases. For $N\neq 0$, the penetration thickness is of order of K^{-1} and can be estimated from Eq. (8). Using the fact that $\Omega_r\sim k$, one finds, for $N\gg 1$:

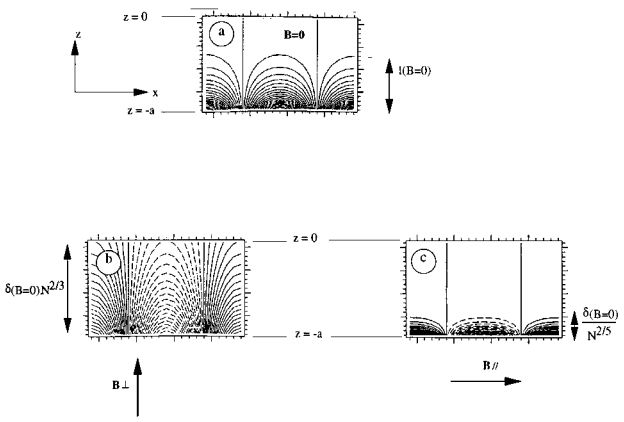

FIG. 14. Influence of the direction of B on the streamlines penetration in the liquid metal (a) $B=0$, (b) B is perpendicular to the sheet and $N=10$, (c) B is parallel to the sheet and $N=10$.

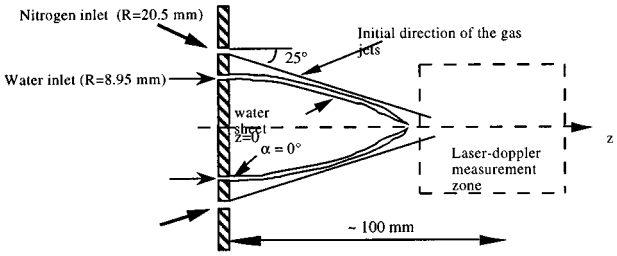

FIG. 15. Disintegration of a water sheet by a nitrogen flow.

$$\frac{\delta(B_\perp)}{\delta(B=0)}=\frac{K_\perp^{-1}}{k^{-1}}=\left(\frac{\Omega_{i\perp}}{N}\right)^{-1/2}=f(\mathrm{We},\rho,\Delta V)N^{2/3}, \quad (26a)$$

$$\frac{\delta(B_\parallel)}{\delta(B=0)}=\frac{K_\parallel^{-1}}{k^{-1}}=\left(\frac{\Omega_{i\parallel}}{N}\right)^{1/2}=g(\mathrm{We},\rho,\Delta V)N^{-2/5}, \quad (26b)$$

where δ denotes the typical dimensionless penetration length of the instability into the metal layer.

The unperturbed velocity and the mean thickness of the liquid-metal sheet have been assumed to be unaffected by the magnetic field in the above section. This hypothesis is fully valid for the case of a parallel magnetic field where no braking force is generated along the x direction. On the contrary, a braking forces appears when the magnetic field is perpendicular to the sheet, which will be responsible for a decrease in velocity and a thickening of the liquid sheet. The quantity $U_0 a$ will remain a constant owing to the mass conservation. This relation, together with Eq. (8) shows that these modifications of the sheet properties will produce an increase in N and a decrease in We. For a perpendicular magnetic field Table I shows that these changes yield a decrease in $\Omega_{i\ \max}$, and as a consequence the value of $\Omega_{i\ \max}$ in Fig. 12 is overestimated. One can conclude that the effect of the braking force on the unperturbed liquid metal layer is an additional reason for the braking of the instability development.

IV. EXPERIMENTAL RESULTS FOR $B=0$

An experimental setup was built to validate the results in the pure hydrodynamic situation, i.e., with $N=0$ (Fig. 15). While experiments with a liquid metal sheet and with a magnetic field would be of great interest, the technical difficulty of applying a magnetic field around the entire sheet and the severe health problems arising in the atomization of a mercury sheet by violent gas streams have not yet been overcome. An axisymmetrical water sheet was created by a nozzle consisting of a 100 μm annular slot having a mean radius of 8.95 mm. The initial angle of the water sheet was zero with respect to the horizontal direction. An external coaxial nitrogen flow was provided by another concentric slot having a thickness of 1.13 mm and a mean radius equal to 20.5 mm. The initial angle of the gas flow was equal to 25° toward the z axis representing the horizontal direction. Hereafter, $z=0$ will denote the location of the vertical plane containing the two concentric annular slots which deliver the water and nitrogen flows. The water flow rate is controlled by a flowmeter. A set of 36 pressurized nitrogen tanks feeds the gas nozzle via a regulating valve to control the pressure.

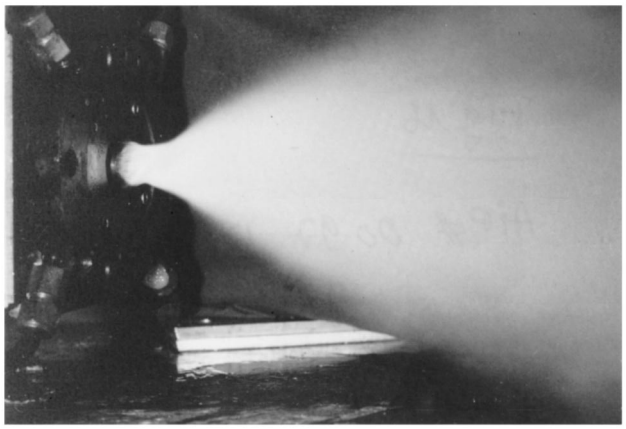

FIG. 16. Visualization of the spray.

A Pitot tube was used to measure the gas velocities in the atomization zone. These measurements, together with shadowgraphic and strioscopic visualizations showed that the gas stream first converged under the effect of the initial angle at the nozzle outlet (25°), and, then, diverged in a plume-like pattern (see Fig. 16). For a given value of z, a radial sweep of the gas velocity measurements showed that the flow was actually confined to a relatively narrow annular zone whose radial thickness increases slowly with z. For a given upstream gas pressure $P=11\times10^5$ Pa, Fig. 17 shows the location, in the (r,z) plane, of the points where the maximum gas velocities have been measured. Nevertheless, the general shape of the profile was not strongly affected by using lower input pressures. At $z=25$ mm, Fig. 18 shows an example of the velocity distribution along a radius. In this graph, the velocity has been normalized by the sound velocity $(\kappa RT)^{1/2}$, which is equal to 352 m/s for nitrogen at room temperature with a ratio of specific heats $\kappa=1.4$ and a gas constant $R=296$ J/Kg K.

For a given liquid flow rate, the water sheet has a profile $r(z)$ which can be easily calculated following the method described by Gasser and Marty.[4] Figure 19 shows the evolution of these profiles for various water flow rates and without gas flow. Although these mean water profiles will be affected by the gas flow, the interaction between the liquid sheet and the gas stream probably occurs in the region $z\sim10-20$ mm where the radial distance between them is minimum as shown in Figs. 17 and 19. This region has been indicated in

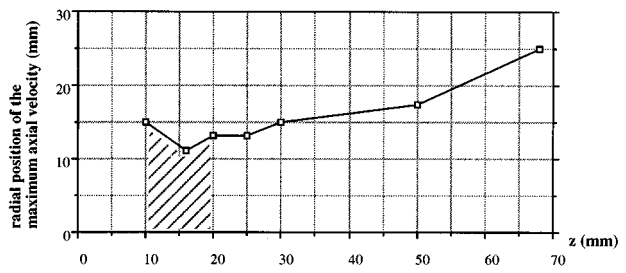

FIG. 17. Radial location of the maximum axial velocity of the gas jet for an upstream gas pressure $P=11\times10^5$ Pa. The hatched zone denotes the location where interaction between the gas flow and the liquid sheet is expected to occur.

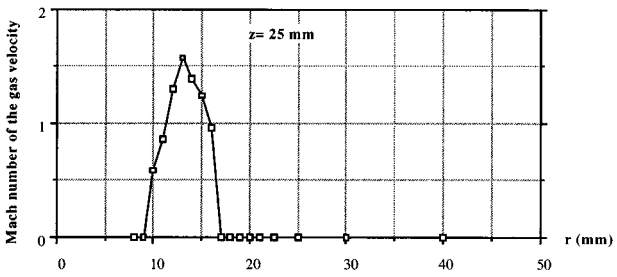

FIG. 18. Radial profile of the gas axial velocity at $z=25$ mm.

Fig. 19. Therefore, the axial position at $z=100$ mm is suitable for measuring the sizes and velocities of the water drops constituting the spray. To do so, a Phase-Doppler-Particle-Analyzer (PDPA) has been installed on a horizontally moving table, allowing a radial exploration of the spray at $z=100$ mm (Fig. 20). For a pressure $P=4\times10^5$ Pa upstream from the gas nozzle and a water flow rate $Q=1.66\,l$/mn, Fig. 21 shows the radial evolution of the diameters D_{10} and D_{30} from $r=20$ to 80 mm (the mean diameters D_{10} and D_{30} are defined as: $D_{10}=(1/N)\Sigma_{i=1}^{N}d_i$ and $D_{30}=\Sigma_{i=1}^{N}(d_i^3/N)^{1/3}$. The run time was typically 5 s corresponding to around 1000 measurements). Their averaged values are $D_{10}\sim21\ \mu$m and $D_{30}\sim26\ \mu$m. There is a slight increase of the diameter D_{10} of the particles as the measurement volume is displaced toward larger radii. This trend has also been found in an experimental study of coaxial-jet injectors for rocket engines.[11] In this latter study, the size measurements were made with a Malvern diffraction particle sizer. This evolution of the particle size with increasing radius was also found by Gomi[12] (1984). This observation was also mentioned in an experimental study of the atomization of a cylindrical water jet[13] in which the drop size measurements were also made with a Malvern particle sizer. A knowledge of the gas velocity is also needed in order to validate the first part of the present results. The results obtained with the Pitot tube have been verified with laser measurements by assuming that the velocity of the smallest droplets found in the spray (a few microns) was roughly equal to that of the nitrogen flow. Figure 22 shows the radial profile of this velocity whose mean

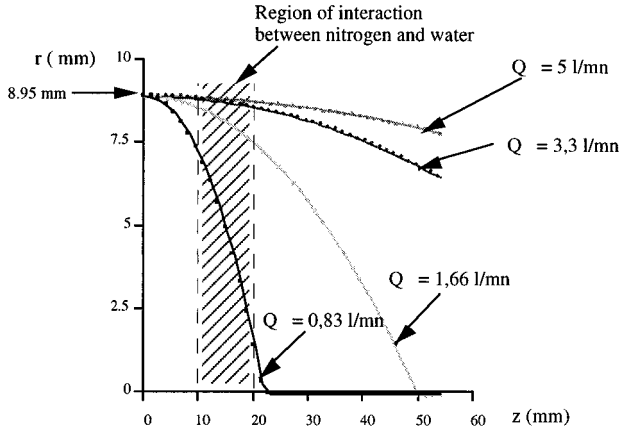

FIG. 19. Calculated water sheet profiles for various liquid flow rates without gas flow.

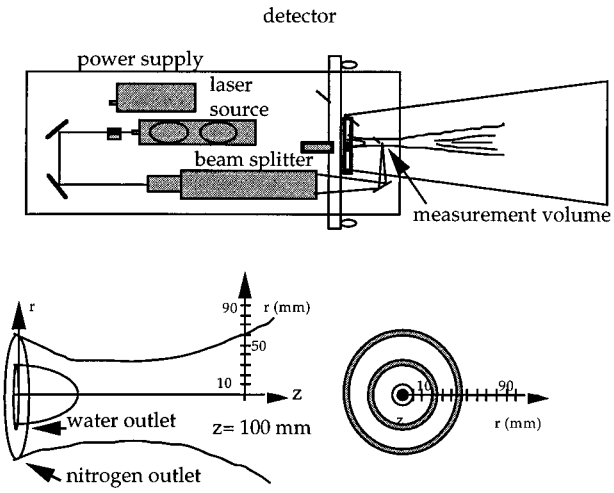

FIG. 20. Equipment for laser-doppler measurements at $z=100$ mm.

value is approximately equal to 125 m/s for our experimental conditions. (Only dimensional quantities are used in this section. Nevertheless, with a velocity equal to 125 m/s, and with $a=100\ \mu$m for the characteristic water film thickness, the Weber number We$\sim$28.) This value, together with the density $\rho_g=1.25\ \mathrm{kg\,m^{-3}}$ of the gas and the value $\gamma=0.073\ \mathrm{Nm^{-1}}$ of the interfacial tension between water and nitrogen, are needed for the calculation of the wavelength, say λ_1, of what can be considered as the primary instability. Neglecting the liquid sheet velocity with respect to that of the gas, this wavelength can be deduced from Eq. (11):

$$\lambda_1=\frac{2\pi}{q}=\frac{2\pi\gamma}{\rho_g(\Delta U)^2}=23.5\ \mu\mathrm{m}. \tag{27}$$

The nonlinear evolution of the primary instability leads to rolls which are transformed into ligaments before disintegrating into droplets. This stage is often referred to as the secondary instability. A first theoretical attempt to determine the diameter of these droplets could be based on the assumption that the leading mechanism of disintegration of the ligaments is the Rayleigh instability, in which the more rapidly growing modes have a wavelength, λ_{Ral}, approximately equal to 9 times the radius of the ligament (see Chandrasekhar[14]). Assuming that the diameter of the ligaments is half the primary wavelength (i.e., $\lambda_1/2$), we obtain: $\lambda_{\mathrm{Ral}}\sim 9\lambda_1/4$. Assuming also that the segment of ligament which will be produced by the Rayleigh instability will be totally converted into a sphere of diameter d_s, one finds:

$$\lambda_{\mathrm{Ral}}\,\frac{\pi}{4}\left[\frac{\lambda_1}{2}\right]^2=\frac{4}{3}\,\pi\left[\frac{d_s}{2}\right]^3. \tag{28}$$

The value $d_s=22.2\ \mu$m of the diameter of the spheres which is deduced from Eq. (28) is surprisingly very close to the diameter D_{10} obtained experimentally. Nevertheless, owing to the high gas velocity around the ligaments, the Rayleigh instability is probably not a good mechanism for explaining the secondary breakup.

Another way of estimation of the final size of the droplets produced in our experiment is to refer to a breakup map such as that proposed by Hsiang and Faeth[15] in a detailed

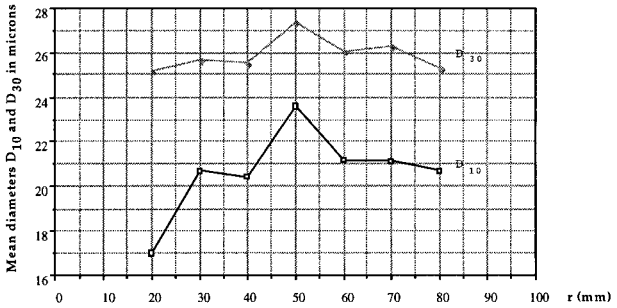

FIG. 21. Radial distribution of the mean diameters D_{10} and D_{30} for an upstream gas pressure $P=4\times10^5$ Pa and a liquid flow rate $Q=1.66\ l$/mn.

study of the deformation and breakup of a liquid drop. For small values of the Ohnesorge number [Oh $=\mu_L/(\rho_L d_0\gamma)^{1/2}$, representing the ratio of liquid viscous and drag forces to surface tension forces], the authors[15] showed that the transition between an oscillatory regime (which does not divide the drop) and the so-called ''bag breakup'' (which leads to the drop destruction and its disintegration into a wide number of smaller drops) was occurring when the Weber number, We, based on the diameter of the drop, was approximately equal to 10. For a drop size d_0 approximately equal to 25 μm in our case, and a value $\mu_L=10^{-3}\ \mathrm{Kg\,m^{-1}\,s^{-1}}$ for the dynamic viscosity of water, we find that Oh$\sim2\times10^{-2}$. Consequently, the critical value We $=10$ applies to our experiment and the diameter, d, of the water drops constituting the spray for our working conditions should be such as:

$$\mathrm{We}=\frac{\rho_g U^2 d}{\gamma}=10. \tag{29}$$

Given the velocity $U=125$ m/s of the nitrogen flow, this expression yields a value $d=37\ \mu$m, approximately 50% higher than our experimental findings. A possible explanation for this difference could be that the typical size of the initial structures produced by the primary instability would be so large that the actual We is much greater than 10. In this case, after Hsiang *et al.*,[15] this situation was observed to give rise to a ''multimode breakup'' which produces a wide variety of drop sizes, including very fine droplets (see Krzeczkowski[16] for photographs of this regime).

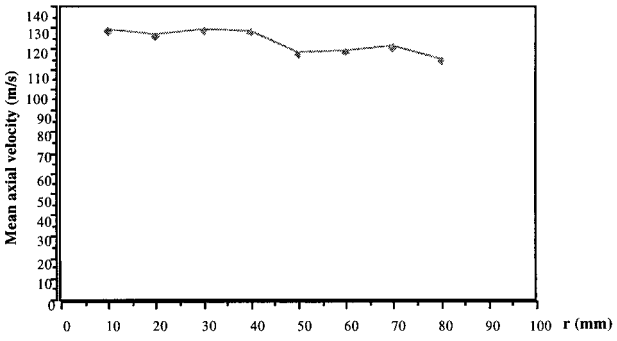

FIG. 22. Radial distribution of the velocity of the smallest droplets in the spray at $z=100$ mm.

V. CONCLUSION

In the first part, a linear stability study of a two-dimensional liquid sheet of metal sandwiched between gas flows has been presented. The effect of a magnetic field has been studied according to its orientation with respect to the sheet. The wave numbers of maximum temporal growth rate have been found to scale with We $(\Delta V)^2$, independently of the direction or intensity of the magnetic field. When We$\gg$1, it has been shown that the growth rate Ω_i of the instability is decreased when a perpendicular magnetic field is applied. An opposite effect has been observed with a parallel field. An explanation based on the modification of the penetration depth of the hydrodynamic streamlines in the liquid metal has been proposed. This explanation takes into account the effect of inertia of the fluid involved in the instability on the growth rate. In the asymptotic case of high interaction parameters ($N\gg1$), analytical expressions of the maximum growth rate $\Omega_{i\,\max}$ have been obtained and compared to numerical results.

Experimental results obtained by atomization of a conical water sheet with a nitrogen flow have been presented. Although conducted for a particular set of values of the various parameters, the particle size measurements are in global agreement with the first part of this paper, suggesting that the dependence of the drop size, d, with the gas velocity, U_g, follows a U_g^{-2} power law. This is in agreement with other experimental works made on circular liquid jets atomized by a coaxial circular gas flow (see Hopfinger and Lasheras,[13] 1994 or Ledoux *et al.*,[11] 1995 for example).

ACKNOWLEDGMENTS

The authors gratefully acknowledge financial support from the Direction des Recherches et Etudes Techniques (DRET) and fruitful discussions with Dr. J. C. Gasser. The experimental tests have been made by T. Erikson. Dr. A. Cartellier from LEGI is thanked for advice concerning the laser-Doppler measurements. One part of the experimental facility has been lent by Professor F. Bark from the Royal Institute of Technology in Stockholm.

APPENDIX: COEFFICIENTS OF THE DISPERSION EQUATION

The coefficients α_i of Eq. (10) are:

$$\alpha_0=-(V_1^2+V_2^2)\,\frac{k}{K}\,\rho(\coth(2K))+2\,\frac{k^2}{K}\,\frac{\rho}{\mathrm{We}}\,(\coth(2K))-\frac{k^2}{K^2}\,\rho^2-\frac{k^2}{\mathrm{We}^2}-V_1^2V_2^2+\frac{k}{\mathrm{We}}\,(V_1^2+V_2^2)+\frac{1}{k^2\mathrm{Fr}^2}+\frac{1}{\mathrm{Fr}k}\,(V_1^2-V_2^2),$$

$$\alpha_1=2(V_1^2+V_1+V_2^2+V_2)\,\frac{\rho}{K}\,(\coth(2K))-4\,\frac{k}{K}\,\frac{\rho}{\mathrm{We}}\,(\coth(2K))+4\,\frac{k}{K^2}\,\rho^2+\frac{2}{k}\,(V_1+V_2)V_1V_2-2\,\frac{(V_1+V_2)}{\mathrm{We}}+\frac{2}{\mathrm{Fr}}\,\frac{(V_2-V_1)}{k^2},$$

$$\alpha_2=-(2+V_1^2+V_2^2+4V_1+4V_2)(\coth(2K))\rho\,\frac{1}{kK}+\frac{2}{K}\,\rho\,\frac{1}{\mathrm{We}}\,(\coth(2K))-6\rho^2\,\frac{1}{K^2}-\frac{1}{k^2}\,(V_1^2+V_2^2+4V_1V_2)+\frac{2}{k\mathrm{We}},$$

$$\alpha_3=\frac{(4+2V_1+2V_2)\coth(2K)\rho}{k^2K}+\frac{4\rho^2}{kK^2}+\frac{2(V_1+V_2)}{k^3},$$

$$\alpha_4=-\frac{1}{k^4}-\frac{\rho^2}{K^2}-2\rho\,\frac{\coth(2K)}{Kk^3}.$$

[1] A. D. Sneyd, ''Stability of fluid layers carrying a normal electric current,'' J. Fluid Mech. **156**, 223 (1985).

[2] R. Moreau, S. Pigny, and S. A. Maslowe, ''Amplitude evolution of interfacial waves in aluminium reduction cells,'' in *Liquid Metal Magnetohydrodynamics*, edited by R. Moreau and J. Lielpetris (Kluwer, Dordrecht, 1989).

[3] J. Descloux and M. Romerio, ''On the analysis by perturbation methods of the anodic current fluctuations in an electrolytic cell for aluminium production,'' in Ref. 2.

[4] J. C. Gasser and Ph. Marty, ''Liquid sheet modeling in a swirl atomizer,'' Eur. J. Mech., B/Fluids **13**, 765 (1994).

[5] R. Rivat, J. Etay, and M. Garnier, ''Stabilization of a surface wave by a magnetic field,'' Eur. J. Mech., B/Fluids **10**, 537 (1991).

[6] W. Hagerty and J. Shea, ''A study of the stability of plane liquid sheets,'' J. Appl. Mech. **22**, 509 (1955).

[7] M. V. Panchagnula, P. E. Sojka, and P. J. Santangelo, ''On the three-dimensional instability of a swirling, annular, inviscid liquid sheet subject to unequal gas velocities,'' Phys. Fluids **12**, 3300 (1996).

[8] S. P. Lin, Z. W. Lian, and B. J. Creighton, ''Absolute and convective instability of a liquid sheet,'' J. Fluid Mech. **220**, 673 (1990).

[9] H. B. Squire, ''Investigation of the instability of a moving liquid film,'' Br. J. Appl. Phys. **4**, 167 (1953).

[10] J. C. P. Huang, ''The break-up of axisymmetrical liquid sheets,'' J. Fluid Mech. **43**, 305 (1970).

[11] M. Ledoux, I. Care, M. Micci, M. Glogowski, L. Vingert, and P. Gicquel, ''Atomization of coaxial-jet injectors,'' Proceedings of the Second International Symposium on Liquid Rocket Propulsion, Onera, Paris, 1995 (unpublished).

[12] H. Gomi, ''Pneumatic atomization with coaxial injectors,'' Ph.D. thesis, University of Sheffield, 1984.

[13] E. J. Hopfinger and J. C. Lasheras, ''Breakup of a water jet in high velocity co-flowing air,'' Proceedings of the ICLASS-94 International Conference, Rouen, France, July 1994, (unpublished), pp. 110–117.

[14] S. Chandrasekhar, *Hydrodynamic and Hydromagnetic Stability* (Dover, New York, 1961).

[15] L. P. Hsiang and G. M. Faeth, ''Near-limit drop deformation and secondary breakup,'' Int. J. Multiphase Flow **18**, 635 (1992).

[16] S. A. Krzeczkowski, ''Measurement of liquid droplet disintegration mechanisms,'' Int. J. Multiphase Flow **6**, 227 (1980).